Bio-inspired Knee Joint of a Lower-limb Exoskeleton for Misalignment Reduction

Taeyeon Kim, *Student Member, IEEE,* Mingoo Jeong, *Student Member, IEEE,* and Kyoungchul Kong, *Member, IEEE*

***Abstract*—Misalignment between an exoskeletal robot and the wearer's body must be minimal to prevent injury and discomfort during active assistance. It is particularly difficult for the robot to imitate the knee joint motion of a human because the human knee joint has a complex structure, which cannot be realized with a single revolute joint. In this paper, a knee joint mechanism that closely realizes the human knee joint motion using the curved guide rail and bearings is proposed. For the optimal design of the proposed mechanism, the motions of the tibia and the femur are captured, and the guide rail of the proposed mechanism is designed to realize the captured human knee joint motion. A simulation study is performed based on kinematic calculations, and the shape of the guide rail is optimized for the proposed device to precisely imitate the human motion. This paper also introduces an experimental method for the quantitative evaluation of the misalignment; the pressure inside the brace is measured using an air-pressure sensor pad, and the pressure measurements are utilized for objective comparison of the misalignment with respect to the joint mechanism. An additional experiment is performed to verify the non-interfering of the human walking motion.**

***Index Terms*—Misalignment in exoskeleton, Knee joint mechanism, Bio-inspired joint, Mechanism design.**

I. Introduction

THE human knee realizes peculiar and complex movements by its anatomical structure. During the flexion and extension of the human knee, sliding and rolling occur depending on the shape of the bones and ligaments [1]. According to the human data, the instantaneous center of rotation (ICOR) of the tibia moves significantly in the mid-range of the flexion since the sliding motion that pushes away the ICOR is not negligible. However, many existing exoskeletal robots for augmentation, rehabilitation, or unpowered exoskeletons, such as orthotic devices, have a common assumption that the knee joint is a fixed single revolute joint structure [2]–[7]. The leg of the robot and the human leg construct a closed linkage system connected by the joints and the braces. Since the kinematic solution does not exist because of the different rotation axis and the simplification of the joint mechanism, a misalignment between the exoskeleton and the wearer's body is unavoidable, which becomes even more severe when the wearer moves from the initial posture. This misalignment acts as the main factor of the unintentional repulsive force between the wearer and the robot system, which does not only reduces the actuator's power transmission efficiency but also makes the wearer feel discomfort as the robot is obstructing their movement [8]. Therefore, it is essential to decide the joints' kinematics so that they can precisely reproduce human movements.

The authors are with the Department of Mechanical Engineering, Korea Advanced Institute of Science and Technology (KAIST), 291, Daehak-ro, Yuseong-gu, Daejeon, Republic of Korea (Email: ty.kim, mg.jeong, kckong at kaist.ac.kr). This research was supported by a grant of the Korea Health Technology R&D Project through the Korea Health Industry Development Institute (KHIDI), funded by the Ministry of Health & Welfare, Republic of Korea (grant number: HJ20C0007) and the Technology Innovation Program (20007096) funded By the Ministry of Trade, Industry and Energy (MOTIE, Korea)

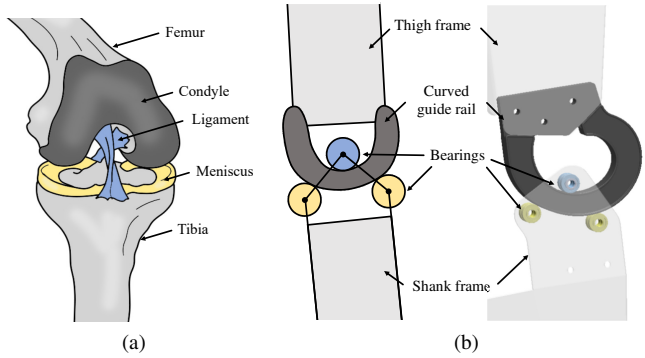

Fig. 1. The basic concept of the proposed joint mechanism that is inspired by (a) human knee anatomy. (b) Schematic diagram of joint mechanism and final 3D design of the bio-inspired joint. The parts which have the same role are represented with the same color.

Recently, various attempts have been made to analyze the motion of the knee joint and apply it to the design of exoskeletal robots. Some of the designs have more than one degree of freedom (DOF), such as a passive pulley, multiple-rolling-cam structure with cable-driven actuators [9]–[12]. These methods do not imitate the human knee joint movement, and the discrepancy in the mechanism and the human knee joint were to be compensated by the mechanical tolerance by a flexible structure. Although it might be helpful to avoid the misalignment issue, however, the flexible structure deteriorated the efficiency of the assistance, because the supportable ground reaction force and torque transfer efficiency may be reduced since the flexible structure can also dissipate the load force to additional degrees of freedom. Wang et al. modeled the femur curve with a combination of ellipses and mechanically reproduce with revolute joints and cam rollers [8]. However, the weight and size may not be suitable for a wearable system.

There are several attempts to imitate the human motion data with single-DOF structures. Kordasz et al. converted the X-ray image and calculated the trajectory of the ICOR of the tibia [13]. Four-bar linkage is proposed to follow these trajectories, and the simulation result is compared with

the actual tibia's movements. Some studies manufactured the mechanical structures and applied them to the exoskeletal robots, for example, implementing a four-bar linkage using the bearing series and a curved surface [14], [15] or applying a gear-connected single-DOF five-bar linkage [16], [17]. It can follow a human trajectory better than a revolute joint, but multiple link lengths have to be optimized simultaneously, and the hardware will be inevitably complicated. In contrast, Terada et al. implemented the ICOR's trajectory using a grooved cam structure instead of linkage structures [18], [19]. They applied it to a rehabilitation exoskeleton by allowing the rotational axis of the shank frame to move along the grooved path. Although the hardware is relatively simple, the ICOR data measured in the studies that are described above have all different shapes and lengths depending on the method of estimating the trajectory. This feature may lessen the reliability of structures by mimicking the movement of the ICOR.

Rather than using the ICOR, a structure that can utilize the tibia's trajectory with respect to the femur need to be devised. A simple, lightweight single-DOF joint system that can support loads and minimizes friction is the goal of this study. This paper introduces a bio-inspired joint that is motivated by the anatomy, especially the femur condyle and the meniscus in a human knee, as shown in Fig. 1. Before introducing each element of the structure and the process of determining the shape, Fig. 2(a) presents an exoskeletal robot to which the proposed knee joint structure is applied. It has four actuators for sagittal plane rotation at both hip and knee. All structures, including joints, frames, and braces, are manufactured to fit the body shape of the wearer, and through this, the increase in weight and inconvenience caused by adding additional devices to be implemented for general versatility can be eliminated as much as possible. It is a wearable system designed for human augmentation, thus high-speed mobility should also be considered. Therefore, unlike exoskeletal robots in which knees are implemented with the revolute joint mentioned above, misalignment at high speeds can adversely affect the wearer, so a structure that can precisely follow the movement of the knee is essential.

The remaining part of this paper is constituted as follows. Section 2 shows a bio-inspired joint structure based on the generated curve. Section 3 explains how to calculate and optimize the trajectory curve and to confirm the feasibility through kinematic calculation. The experimental result using a whole-body exoskeletal robot is introduced in section 4. A sensor system at the brace which can measure the unintended reaction pressure between the wearer and the robot is suggested, and a comparison with revolute joints using the same robot has also been discussed. Finally, a summary of the paper and proposed directions for future work are listed in section 5.

II. Design of the Bio-inspired Joint

The meniscus is crescent-shaped cartilage attached to the tibia, located on the medial and lateral sides of the knee joint as shown in Fig. 1(a). The outer edge is thicker than the inside, so it is concave at the lateral view. This outer edge keeps the femur's rounded bottom in place, preventing excessive

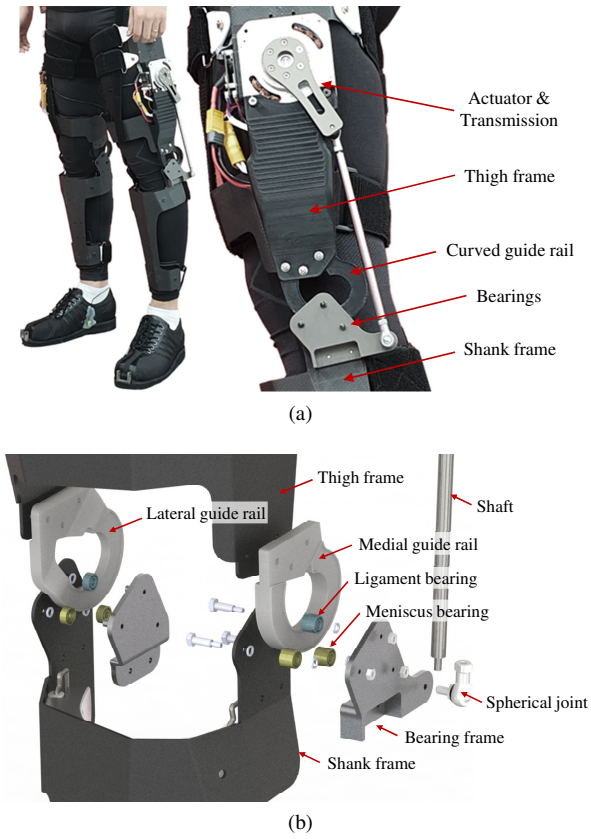

Fig. 2. The lower-limb exoskeletal robot that the proposed knee joint mechanism is utilized. (a) A human subject wears an exoskeletal robot. (b) Exploded view of the proposed joint structure for both medial and lateral side.

dislocation of the tibia and femur. Furthermore, a meniscus serves to distribute the body weight and reduce friction during movements.

As briefly mentioned earlier, two types of basic movement occur between the femur condyle and the meniscus. The first basis is rolling at the contact point, and the other is sliding in the tangential direction passing through the contact point. These two bases form a two-dimensional state plane and determine the 2DOF relative position between the condyle and the meniscus at some moment. However, the actual knee movement has less DOF in the sagittal plane. The bent knee angle can be considered as an injective function in which the domain is a relative position between the femur and the tibia. It means that the joint movement can be reproduced with a single DOF rather than two. Based on the above aspect, the mechanism by which the bearings glide along the guide rail, such as the femur condyle and the meniscus, can replace the tibiofemoral joint as displayed in Fig. 1(b).

The curved guide rail is fastened to the thigh frame, like a condyle attached to the femur. The bottom of the rail is contacted with two bearings [see the yellow-colored components in Fig. 1], which act like the meniscus. Based on the direction of the wearer, these bearings are named as front meniscus bearing $B^{\mathrm{F}}_{\mathrm{Me}}$, and the rear meniscus bearing $B^{\mathrm{R}}_{\mathrm{Me}}$. Another bearing [see the blue ones in Fig. 1] acts as ligaments that prevent separation between the femur and the tibia contacts at the top of the rail, so it was named as ligament bearing

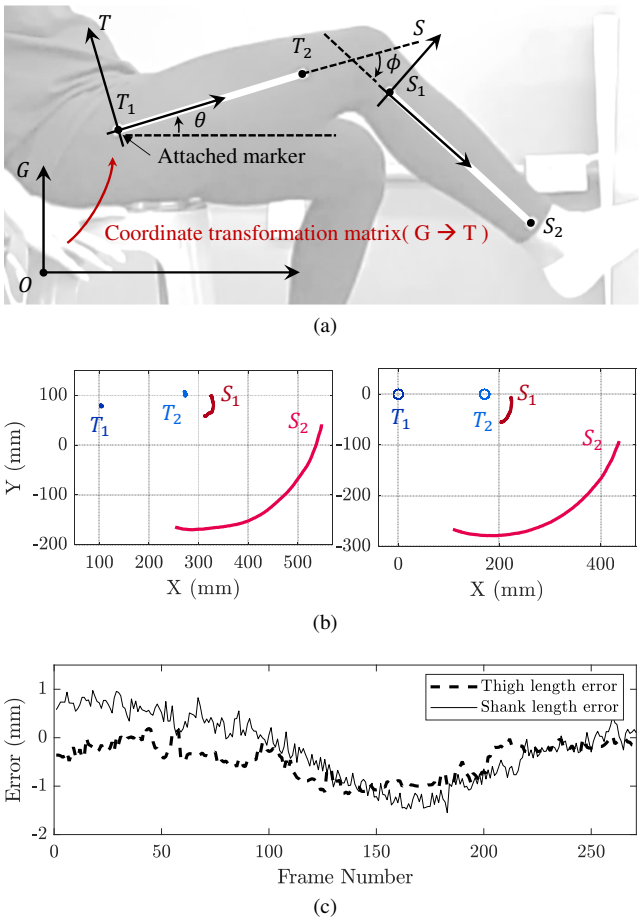

Fig. 3. Data extracting process. (a) A snap-shot of a video clip which the subject with markers is filmed, and coordinate by each marker position (T_1, T_2, S_1, and S_2). (b) Re-calculated position data of four markers by coordinate transformation. (c) Distance value error between markers of thigh and shank extracted from the snap-shot images.

B_{Li}. The upper curved surface was calculated later so that the three bearings always maintain three-point contact with the guide rail surface.

Detailed structure is described with an exploded view in Fig. 2(b). The shapes of the medial and lateral guide rails are slightly different. The medial guide rail has bent through the knee and placed inside of the shank frame. The thickness has also been minimized so that it does not touch the wearer's skin inside the frame. This design eliminates the protrusion to the medial side, prevents collision with two legs when walking or running. It is required to set a goal to designing slim hardware since even if they may not collide with each other, the wearer who perceives the presence of abnormal protrusions causes unnatural movements.

III. Curvature Optimization and Simulation

A. Data Extracting and Curve Fitting Process

Position data of the femur and the tibia are utilized to determine the shape of the guide rail. First, the markers attached to the subject's body were filmed, and the markers' positions at each time frame were extracted via motion tracking. Two markers for each segment can fully explain the femur and tibia's motion in the sagittal plane. The two markers at the thigh are named as T_1 and T_2, and same manner at the shank, S_1 and S_2, as shown in Fig. 3(a).

The coordinate systems T and S are defined for a position rearrangement through the coordinate transformation. The origin of coordinate T is set as T_1, and the x-axis is defined as it passes through T_1 and T_2, and in the same manner at the shank as coordinate S. So each frame T and S are attached to the femur and the tibia, respectively. The tibia's movement with respect to the femur is necessary to determine the curved guide rail's shape that acts as a joint. Therefore, the positions of S_1 and S_2 with respect to the ground coordinate G are transformed with respect to the coordinate T. Fig. 3(b) displays the positions that are transformed. In addition, in order to verify the accuracy of the data obtained by image capture, the length errors that may occur during the data extracting from a video clip were obtained in Fig. 3(c). Since the distance between the markers attached to the subject does not change in the real environment, the difference by subtracting the actual value from the estimated value is calculated. It was confirmed that the magnitude of the error value is around 2 mm, and considering that the actual distance between the markers is about 200-250 mm, this data extracting method can be suggested as reliable.

Fig. 4 explains the optimizing process of bearing location. Based on the shank movement, the trajectories of three bearings can be calculated geometrically if their locations are fixed with respect to coordinate S. However, as briefly shown in Fig. 4(a), the trajectories of $B^{\mathrm{F}}_{\mathrm{Me}}$ and $B^{\mathrm{R}}_{\mathrm{Me}}$ will not coincide if the locations of them are randomly selected. Fig. 4(b) shows the example result of two arbitrarily located bearings. It was presented that two different red and blue trajectories are generated. To realize the concurrent contact of two bearings acting like a meniscus and accurately to imitate the human knee movement, their position should be optimized that makes two trajectories almost overlap. In this paper, a bottom curve of the guide rail is optimized on the following hypothesis; Some pair of bearing positions will exist, such that two trajectories will merge into one curve within a negligible amount of error. Four-dimensional brute-force search is done for comparing RMS error between the trajectories at all possible positions. As demonstrated in Fig. 4(c), the error calculating is performed with the iterative scanning of the $B^{\mathrm{R}}_{\mathrm{Me}}$'s position in x-y coordinates. In each iteration, an internal scanning is also performed to find $B^{\mathrm{F}}_{\mathrm{Me}}$ with minimizing RMS error. The optimized position of $B^{\mathrm{R}}_{\mathrm{Me}}$ can be found by pick the point which has the global minimum of RMS error as displayed in Fig. 4(d) after the whole scan process.

In order to utilize the curve for the fabrication of a mechanical guide included in the proposed joint mechanism, an additional process is necessary for a smooth curve. As the marker data include noise due to the resolution issue of the snap-shot images as shown in Fig. 3(c) and Fig. 5, the curve obtained by strictly interpolate the marker data may include noise as well, which results in a rough edge. This may cause an unnecessary fluctuation and large friction if fabricated without the smoothing process.

Thus, the marker data are re-sampled in the polar coordinate

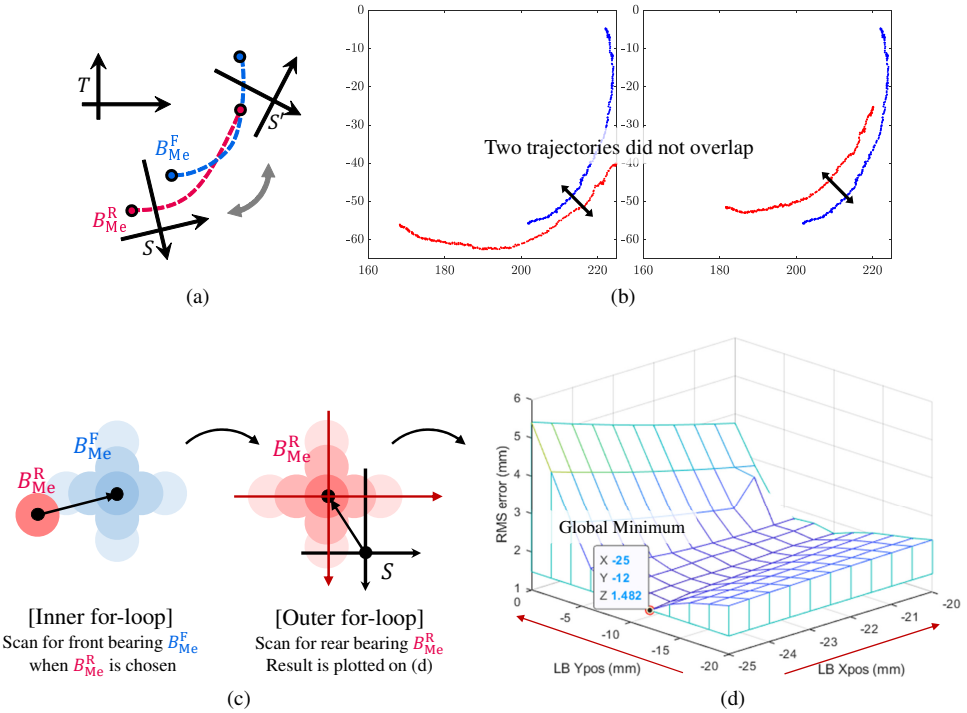

Fig. 4. Meniscus bearings position optimizing process. (a) Schematic diagram showing the trajectories of the two meniscus bearings that are follows the shank coordinate's movement. (b) Arbitrarily located bearing's example result. (c) Four-dimensional scanning of the bearing position (d) and its result. The global minimum, which leads to optimized bearing positions, can be found.

system such that the remapped data have the constant theta interval. Namely, the data is converted from a two-dimensional vector $\mathbf{v}_i = [x_i \;\; y_i]^{\mathrm{T}}$ for $i = 1, ..., N$, where x_i and y_i is the x-coordinate and y-coordinate of the marker position at the Cartesian coordinate system, and N is the number of samples, to $C(\theta_k)$, where

$$\theta_k = \theta_0 + \frac{k}{n}(\theta_l - \theta_0). \tag{1}$$

n is the number of re-sampled data, and θ_0 and θ_l are the initial and final angles, respectively. For any k, $C(\theta_k)$ represents the distance from the fictitious center of rotation $\mathbf{O}_F$ to the edge at the given angle. The position of $\mathbf{O}_F$ for transforming to the polar coordinate system can be found by the least square error circle fitting method. Let's define a circle equation in the Cartesian coordinate system as

$$x^2 + y^2 + a_1 x + a_2 y + a_3 = 0, \tag{2}$$

then define a vector $\mathbf{x} = [a_1 \;\; a_2 \;\; a_3]^{\mathrm{T}}$. The matrix equation from a least square method can be formulated as

$$\mathbf{x} = (\mathbf{A}^{\mathrm{T}}\mathbf{A})^{-1}\mathbf{A}^{\mathrm{T}}\mathbf{b}, \tag{3}$$

where $\mathbf{A}$ and $\mathbf{b}$ are

$$\mathbf{A} = \begin{bmatrix} \mathbf{v}_1 & \mathbf{v}_2 & \dots & \mathbf{v}_n \\ 1 & 1 & \dots & 1 \end{bmatrix}^{\mathrm{T}} \in \mathbb{R}^{n\times 3}, and \tag{4}$$

$$\mathbf{b} = -\begin{bmatrix} |\mathbf{v}_1|^2 & |\mathbf{v}_2|^2 & \dots & |\mathbf{v}_n|^2 \end{bmatrix}^{\mathrm{T}} \in \mathbb{R}^{n\times 1}. \tag{5}$$

Thus the fictitious center of rotation will be an origin point of the fitted circle, which is derived as

$$\mathbf{O}_F = [a_1 \;\; a_2] \,/\, 2. \tag{6}$$

With the re-sampled data in the polar coordinate system, a smooth curve equation for the fabrication of the proposed knee joint mechanism can be obtained by a least-square curve fitting method with a third-degree polynomial, i.e.

$$C_{\mathrm{fit}}(\theta) = \sum_{j=0}^{3} p_j \theta^j. \tag{7}$$

The parameters, p_j, are obtained such that the squared errors between the re-sampled data, $C(\theta_k)$, and the spline curve is minimum. A higher degree of the equation will make less error but definitely cause unnecessary fluctuation. Thus, the order of the function is set as minimum as possible because the curve will be over-fitted to the original data to reduce the RMS error.

As the radius of bearings is fixed, the bottom curve of the guide rail can be calculated as Fig. 6 by offsetting the merged optimal trajectory curve function $C_{\mathrm{fit}}(\theta)$ at the Cartesian coordinate system. The detail of calculating the offset trajectory is explained below. Let's look at some voluntary $(k-1)$th and kth positions of the shank movement. The center of the bearing at θ_{k-1} is B and will be moved to B' at the angle θ_k. B_{M} is the midpoint of these two points. Then the offset trajectory can be obtained by interpolating the all $B_{\mathrm{offset,k}}$ which can be derived as below;

$$B_{\mathrm{offset}} = \left(B_{\mathrm{M},x} \pm r_{\mathrm{P}} \cos\psi, B_{\mathrm{M},y} \pm r_{\mathrm{P}} \sin\psi\right), \tag{8}$$

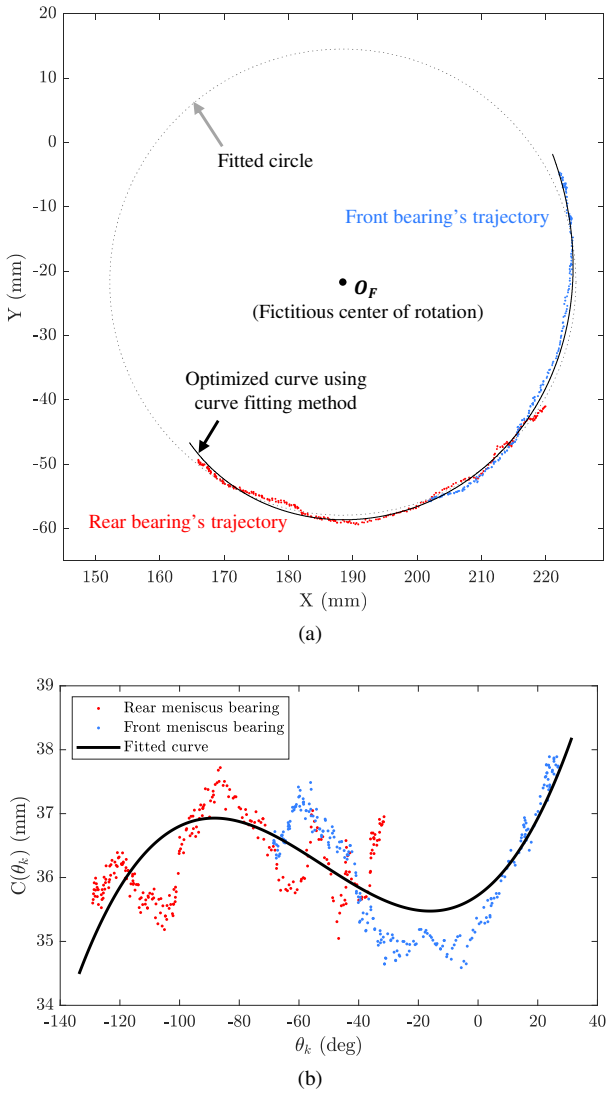

Fig. 5. Optimized bearing trajectories are calculated with the position according to frame S. (a) Curve fitting result represented in the Cartesian coordinate system. (b) Curve fitting result at the polar coordinate system to minimize the error between the curve and the trajectories.

where the direction angle ψ of vector $B_{\mathrm{M}}B_{\mathrm{offset}}$ is

$$\psi = \arctan\left[\frac{-(B'_x - B_x)}{B'_y - B_y}\right], \tag{9}$$

as the subscript x and y means the x-coordinate and y-coordinate value, respectively. Thus, the shape of the curved guide rail that is shown in section 2 can be designed by offsetting two dotted lines in Fig. 7. One of the dotted lines, which represents the trajectory of the ligament bearing, is calculated by the geometric information with respect to the meniscus bearings.

B. Misalignment Calculation

In this section, the conventional revolute joint and the bio-inspired joint proposed in this paper are compared through kinematic simulations. For quantitative comparison, the exoskeleton's two points S_1^{E} and S_2^{E} that are corresponding to the two markers S_1 and S_2 of the subject's shank are defined. If

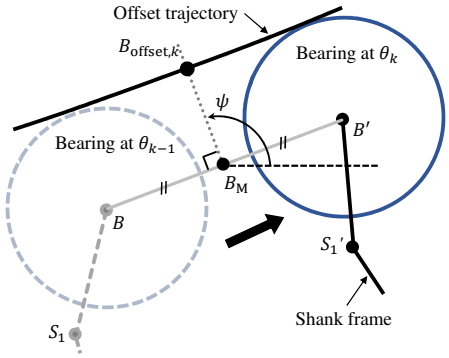

Fig. 6. Getting the offset trajectory to make the curve which maintains contact with bearings.

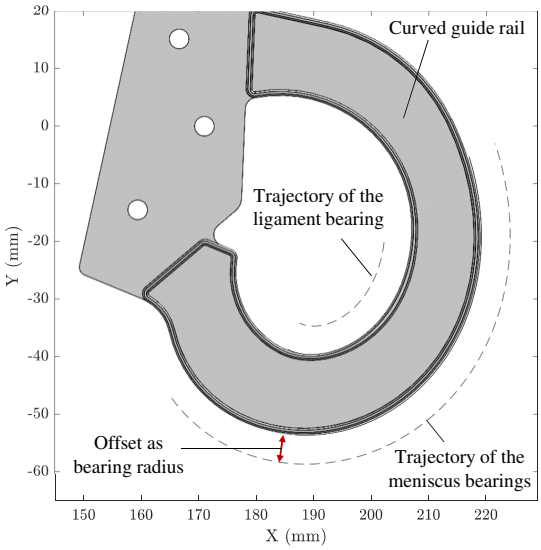

Fig. 7. Simulation result of bearing trajectories and overlapped guide rail at section 2. Curve of the guide rail was created by offset two trajectories.

there is ideally no misalignment, then S_1^{E} and S_2^{E} will coincide with S_1 and S_2. The simulation settings of the comparable revolute joints are described below; The revolute joint is located in the fictitious center of rotation in Fig. 3(a), since the circle fitting has the same idea with truncating the shank movements to a single revolute joint. Then S_1^{E} moves along the circle with radius $|O_F S_1^{\mathrm{E}}|$ at initial state, while generates minimum position error. This ensures a fair comparison to the proposed joint by assuming it is worn in the best conditions achievable with a single revolute joint. Since two situations need to be compared on a predetermined angle vector extracted from the video clip, it is assumed that the wearer's shank and the exoskeleton are parallel to each other at a specific moment and that the length of the exoskeleton part is the same as the subject's without error ($S_1S_2 \parallel S_1^{\mathrm{E}}S_2^{\mathrm{E}}$ and $|S_1S_2| = |S_1^{\mathrm{E}}S_2^{\mathrm{E}}|$). Thus, the position of S_2^{E} can be derived using the position of S_1^{E} and angle of each frame k. Therefore, according to the knee joint angle, the wearer and the exoskeleton will have the same error no matter which marker is selected.

Fig. 8 shows how the simulation works. Fig. 8(a) and Fig. 8(b) is the visualized result of the revolute joint and the bio-inspired joint, respectively. At the bottom left of each plot, the

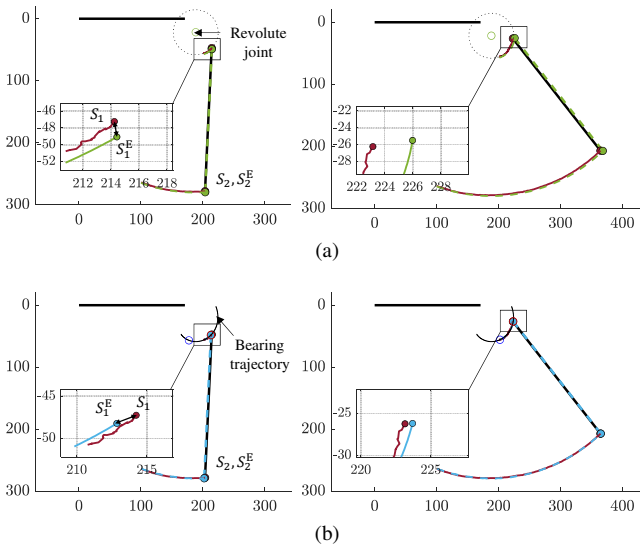

Fig. 8. The captures by time section of the simulation are arranged. It has been calculated and shown how far the exoskeletal robot is with respect to the subject's leg according to the angle. (a) The result of the revolute joint, and (b) the bio-inspired joint.

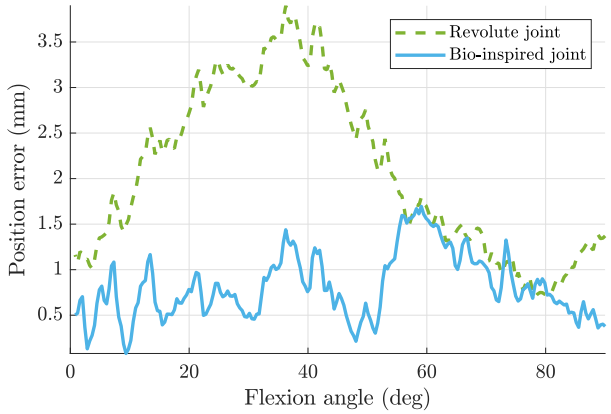

Fig. 9. Position error between the tibia of the subject and the exoskeleton according to knee flexion angles.

exoskeleton's point S_1^{E} and the subject marker S_1 are enlarged for qualitative comparison. The lines are the trajectories of S_1 and S_1^{E}. It is confirmed that there is a difference in the magnitude of the error in the enlarged plot, and the error between the two points is plotted in Fig. 9 for a more intuitive comparison. The error when using the bio-inspired joint is much lower than that of a revolute joint. The total error has been reduced to about 40% compared to the existing revolute joint, and the error level still does not exceed the marker data extraction error, as mentioned with Fig. 3(c). Unlike misalignment caused by using the revolute joint, which fixes the COR position, a slight error between the two curves shown in Fig. 5(b) is the cause of the misalignment that occurs by applying the bio-inspired joint. The high-frequency fluctuation of these errors also seems to be closely correlated with the noise of extracted data.

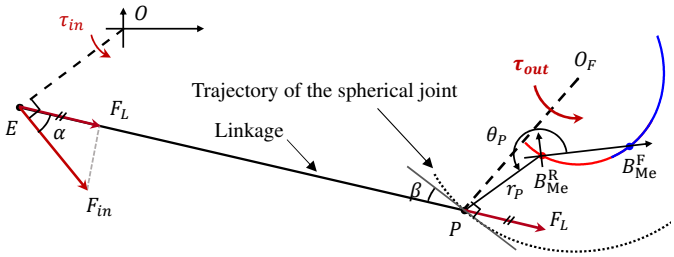

Fig. 10. A kinematic relationship for analyzing the actuation torque transmission ratio of the proposed joint mechanism.

C. Torque Transmission Ratio

Many exoskeletal robots applied the revolute joint at their knee due to the advantage of using the actuator itself as a joint. In contrast, to use the knee joint mechanism proposed in this paper for exoskeletons, actuation power must be transmitted in a unique form. As shown in Fig. 10, a power transmission mechanism similar to the four-bar linkage was selected. The frame O, which is fixed to the thigh frame, has the origin at the center of the knee actuator was defined for solving kinematics. The link OE is the actuator's output link connecting the actuator and the shaft EP. Vertex E and P represent the spherical joint. P is attached to the bearing frame that fixes the three bearings and sliding along through the guide rail. The length of the fictitious link PO_F for calculating the transmitted torque can be described as a function $C(\theta)$ as in section 3-A.

Since the optimal curved trajectory was obtained in the previous section, the positions of the spherical joint E and P can also be expressed as a function of the knee angle. The position of P with respect to the frame O is

$$P = B_{\mathrm{Me}}^{\mathrm{R}} + r_{\mathrm{P}} \left[\cos\left(\theta_{\mathrm{RF}} + \theta_{\mathrm{P}}\right) \quad \sin\left(\theta_{\mathrm{RF}} + \theta_{\mathrm{P}}\right) \right], \tag{10}$$

where the direction angle θ_{RF} between the x-axis of frame O and $B_{\mathrm{Me}}^{\mathrm{R}} B_{\mathrm{Me}}^{\mathrm{F}}$ is

$$\theta_{\mathrm{RF}} = \arctan\left[\frac{B_{\mathrm{Me},y}^{\mathrm{F}} - B_{\mathrm{Me},y}^{\mathrm{R}}}{B_{\mathrm{Me},x}^{\mathrm{F}} - B_{\mathrm{Me},x}^{\mathrm{R}}} \right]. \tag{11}$$

r_{P} and θ_{P} are the norm distance and angle of P in the polar coordinate system which the origin is $B_{\mathrm{Me}}^{\mathrm{R}}$. If the position of P is determined, then the position of E can be derived geometrically. Thus, the positions of the shaft and the output link and the angle between the linkages can be obtained. Using this, the rotation of the knee joint relative to the motor's rotation and the torque transmission ratio to the shank frame can be expressed as a function of several variables. There are four possible variables that can modify; length of the linkages ($|OE|$ and $|EP|$) and position of spherical joint P with respect to the shank frame (r_{P} and θ_{P}). Thus, it is necessary to set up the object of the optimization, and the optimization proceeds accordingly to confirm the structural design of the transmission mechanism.

One of the application that requires high torque at specific angle is running. Kuitunen et al. estimated the joint torque during the ground contact phase in sprinting [20]. In the case of the knee joint, the moment named as τ_{knee} increases after

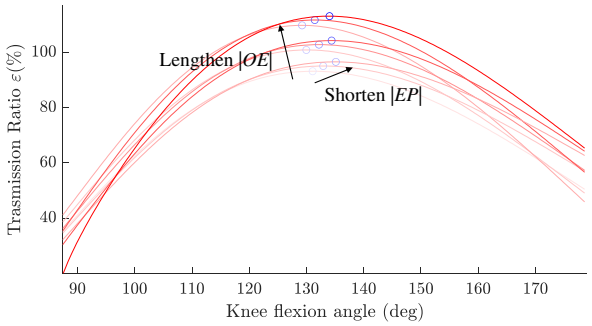

(a)

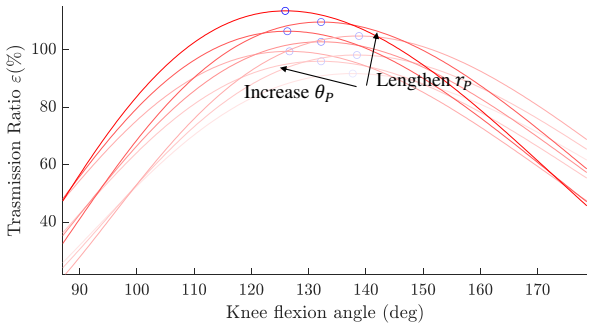

(b)

Fig. 11. Torque transmission ratio to the shank frame. The ratio changes (a) according to the length of each part and (b) position of the spherical joint is shown in the graph.

the touchdown begins at 150°, keep flexing to around 135°until reaching the maximum torque. After passing the peak, the knee is stretched again, and τ_{knee} decreases until taking off at about 155°. The main goal of the optimizing process, therefore, is to maximize the torque transmission and have a peak torque value around 135°.

The torque transmission ratio ε can be derived only with the length information of each link. The motor input torque is named as τ_{in}, then the force F_{in} which produced by the motor and transmitted to the shaft EP is

$$|F_{\text{in}}| = \frac{|\tau_{\text{in}}|}{|OE|} \tag{12}$$

since $\tau_{\text{in}} = OE \times F_{\text{in}}$ and $OE \perp F_{\text{in}}$. The force F_L which is the projection of F_{in} to EP is

$$F_L = |F_{\text{in}}| \cos\alpha \frac{EP}{|EP|} = EP \frac{|\tau_{\text{in}}| \cos\alpha}{|OE||EP|}, \tag{13}$$

where

$$\begin{aligned} \alpha &= \frac{\pi}{2} - \angle OEP \\ &= \frac{\pi}{2} - \arccos\left[\frac{|OE|^2 + |EP|^2 - |OP|^2}{2\,|OE|\,|EP|}\right]. \end{aligned} \tag{14}$$

Thus, the transmission ratio ε between input and output torque, from the motor to the shank frame is

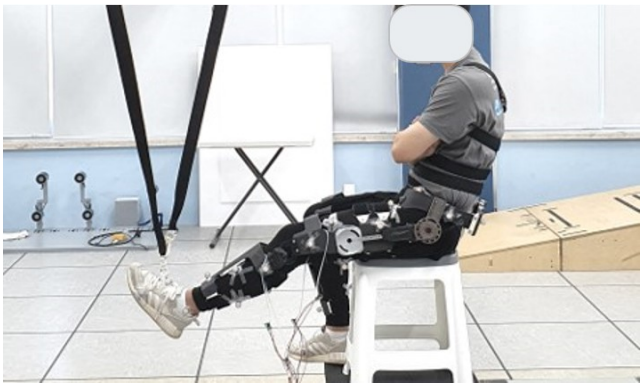

(a)

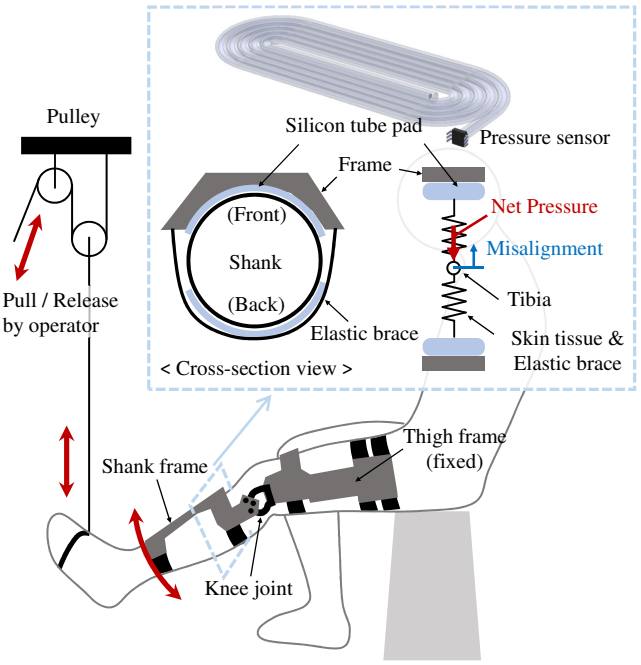

(b)

Fig. 12. Experiment for measuring pressure. (a) Picture of the experiment. (b) Schematic diagram of the experimental procedure and illustration that shows the section view at the shank includes the elastic model by premises.

$$\begin{aligned} \varepsilon_{\text{T}} = \frac{|\tau_{\text{out}}|}{|\tau_{\text{in}}|} &= \frac{|O_F P \times F_L|}{|\tau_{\text{in}}|} \\ &= |O_F P \times EP| \frac{|\tau_{\text{in}}| \cos\alpha}{|OE||EP|} \frac{1}{|\tau_{\text{in}}|} \\ &= \frac{|O_F P|}{|OE|} \cos\alpha \cos\beta, \end{aligned} \tag{15}$$

where

$$\begin{aligned} \beta &= \angle O_F PE - \frac{\pi}{2} \\ &= \arccos\left[\frac{|O_F P|^2 + |EP|^2 - |O_F E|^2}{2\,|O_F P|\,|EP|}\right] - \frac{\pi}{2}. \end{aligned} \tag{16}$$

The variation of the torque transmission ratio at different conditions is plotted in Fig. 11. Blue circles represent the peak point of the transmission ratio, which is drawn by a red line. The cases that have a higher peak point are drawn with

more vivid colors. By adjusting the length of each linkage and position of the spherical joint P, it was possible to change the peak and the overall shape. It suggests that the torque transmitting performance can be optimized to any target angle by changing the length of the transmission system's linkages.

IV. Misalignment Evaluation by Experiment

A. Experiment with Pressure Sensor

This section describes a method and criteria for evaluating the misalignment of an exoskeletal robot using an air pressure sensor pad. A post-processing method for the data extracted through the experiment is also explained. The premise of the experiment is followed. First, the frame of the robot is a rigid body without deformation, and the human skin is an elastic tissue that is deformed according to the appropriate pressure. The elastic velcro braces are also elastic. Second, when wearing the robot in the initial posture, an appropriate amount of pressure must be applied to all parts of the subject's skin.

In this experiment, referring to the shape of the pneumatic sensor used in [21], a pressure measurement module was manufactured by connecting a pressure sensor to an air bladder made of a silicon tube. This module was suitable for measuring interactions between a subject and an exoskeleton since the module can be shaped freely and bend easily. The purpose of this experiment is to measure the misalignment by the manufactured sensor pad. The pressure sensor was chosen to measure the pressure level between the skin and the brace in high resolution. If the area of the silicon bladder is small than the braces, the pressure generated at the remaining area will be ignored. Thus, the entire brace surface must be covered with the pad, so the bladder's shape is selected as the top of the section view in Fig. 12(b).

Muscle activation significantly affects the pressure data. The contraction of muscle fibers changes the cross-sectional shape of the leg with respect to the transverse plane and the physical properties of the muscle. Even if the human subject repeats the same movement, the irregular activity of the muscles must be observed due to several unmeasurable factors, such as fatigue and posture balancing control. Therefore, the deviation range of the overall pressure value will reduce when the movement is performed with muscle deformation as little as possible. In this experiment, passively moving the wearer's body with a pulley operated by another is chosen for minimizing unpredictable muscle activation.

The experiment was conducted as follows. First, attach the sensor pad to both sides of the wearing area. Then, wear the exoskeleton that two types of joint structure are applied, respectively. The robot was worn at the same initial value as the simulation, that is, at the optimal position for each joint. This is to exclude misalignment due to the change of the wearing position, not the type of joint. Next, measure the pressure bias in the initial sitting posture. At last, the pressures from each sensor are measured while repeating flexion and extension via the pulley.

The pressure difference between both sides of the wearing area was obtained through this experiment. Since the skin tissue binding with the brace is modeled to an elastic body as shown in Fig. 12, if the relative position between the wearer and the robot increases, the interaction force generated by the elastic body increases. Therefore, it can be interpreted that the more significant the pressure difference obtained by the experiment, the larger the misalignment. Fig. 13 shows the data obtained from the pressure sensors on both sides of the shank.

For a better understanding of the experimental data, a single experimental result that repeats flexion and extension 5-6 times is shown as a graph in Fig. 13(a) and Fig. 13(b). The top of the three graphs is raw data read from the pressure sensor. Discretization noise caused by the resolution limit and drifting due to the physical properties of the silicon tube bladder can also be observed. The result of filtering to remove these were displayed in the middle graphs. A second-order band-pass filter was used to eliminate noise and drift. The cutoff frequencies were obtained by referring to the flexion and extension period. The graph at the bottom shows the pressure difference ΔP between the two filtered pressure data. ΔP is re-mapped to the angle instead of time and averaged. The maximum pressure value of the revolute joint was measured about 1.4 times higher than that of using the bio-inspired joint. Also, when comparing the sum of the absolute values in the entire section, the bio-inspired joint creates a pressure of only about 70% than the revolute joint. Therefore, through this experiment, it was verified that the bio-inspired joint decreases the pressure when the subject wears the exoskeleton.

One thing that could be discussed is a comparison between the simulated position error and measured pressure that is shown in Fig. 9 and Fig. 13(c). The robot frame's slipping, which occurs in the real environment such as walking or running, makes a difference between the simulation and the experiment. When the misalignment is created, the robot frame will slip to the specific position with the minimum repulsive force since the longitudinal force generated by the misalignment overcomes the friction force from the skin surface. It could be thought that some small limited sliders were added to the shank frame, which affected the joint structure's closed linkage system. Due to the flat shape of the air bladder used in this experiment, it is hard to detect shear force between the skin and robot frame. Thus, the shape of the graph of simulation and experiment can be different.

The range of 0 to 90 degrees of this experiment is the maximum range that can be operated in the experimental environment, and although it is a range sufficient to feel the discomfort of the existing revolute joint, it is narrower than the actual human total range of motion. If analysis is required for motions with a flexion angle of more than 90 degrees, such as squat or running, it is required to use a more advanced measurement method.

B. Verification of No Interference to Walking

Unlike the previous section, which dealt with the results of passive movements, an experiment was additionally performed to compare the gait motions of the subjects before and after wearing the robot. As explained in the introduction section,

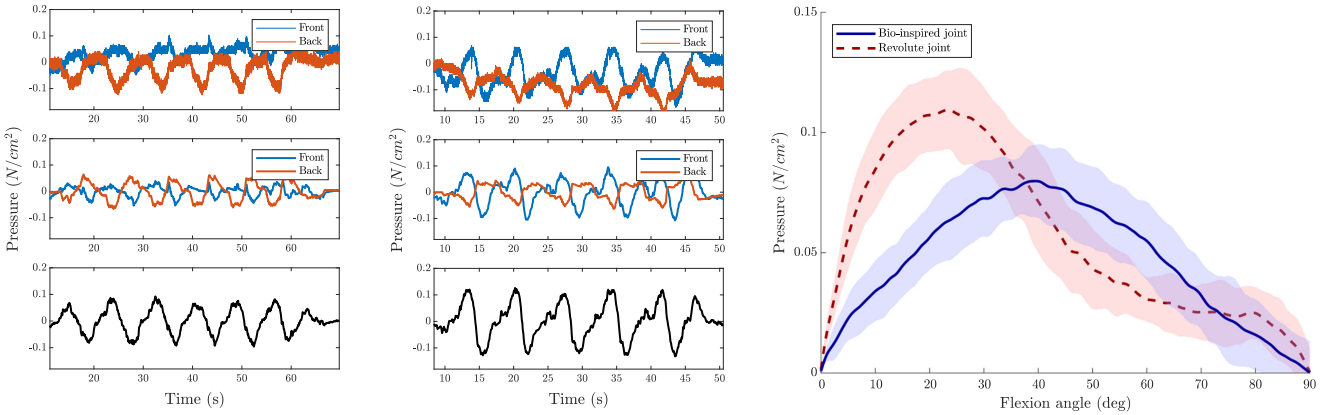

Fig. 13. The pressure measurement result. (a) The pressure of both sides of the shank in the experiment with the bio-inspired joint. (b) Same types of data when the subject wore the revolute joint. (c) The summary of the experiment result. The standard deviation of each data plotted in the faded area.

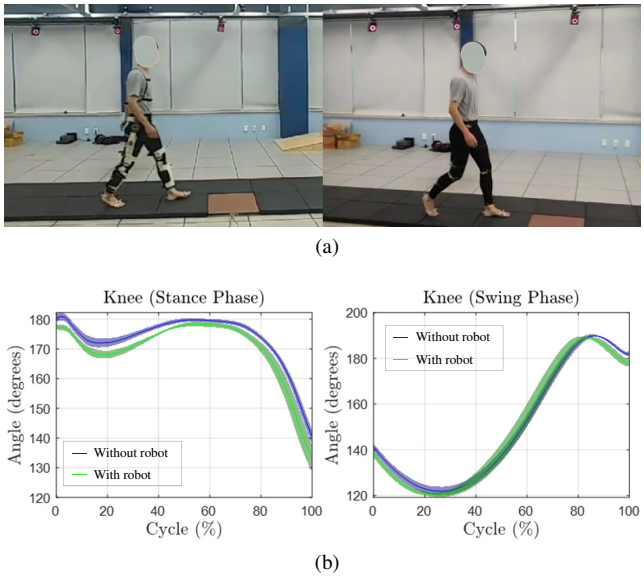

Fig. 14. Experiment for comparing with and without robot frame and joint structure. (a) Picture of the experiment. (b) Knee joint angle plotted in the sagittal plane by motion capture while walking.

if the knee joint mechanism is not well aligned with the human joint, the brace slides or presses the skin. This abnormal move resulting in pain, then the trajectories of the lower limb segments will be changed.

Through 3D motion capture, the movements of the knee joint during walking were measured with and without wearing a robot frame. Subjects were guided to walk a 10 m straight-line at an arbitrary speed, which they felt most comfortable with, and repeated five times for each condition. The knee joint angle was measured and plotted as provided in Fig. 14. It can be seen that two conditions draw consistent plots. Through this, it was confirmed that this joint mechanism does not cause discomfort when wearing.

V. Conclusion

This study devised the design method of a knee joint mechanism that practically reduces misalignment, which is an influential factor that restrains the comfort of the existing lower extremity exoskeletal robot. Curved guide rail and bearings are used to mimic the anatomical structure of the knee joint, such as meniscus and ligaments. The shape of the guide rail is generated from the motion tracking data of the human knee joint by optimizing the position of the bearings at the shank coordinate. Comparing with existing single revolute knee joint was purposed. Position error reducing effect between the wearer and the exoskeleton was verified through kinematic calculation, and the comfort increasing was measured by attaching a pressure sensor pad at the brace. While walking, the robot frame did not interfere the human motion. Additional experiments with more subjects should be done with forthcoming research. The novelty of the bio-inspired design, however, been verified in this paper by fabricating a customized frame and joint for one subject.

Regardless of the field of application, such as medical, military, and industry, the mechanism suggested in this paper can be applied by changing the material or thickness according to the required load condition. Furthermore, this mechanism is not limited to exoskeletal robots. Knee orthosis for arthritis patients, injured people, and the elderly is worn to limit the joint angle or reduce the bodyweight through the patient's knee. Several commercially available products have tried to produce a trajectory similar to the knee joint as much as possible by using different mechanisms with simple and lightweight structures. Among these, the bio-inspired joint, which can limit the joint angle as desired, distribute the body weight, and has a smaller misalignment than any existing orthosis, is considered suitable to be applied to this field.

It can be seen that a new direction for the development of a more comfortable exoskeletal robot was established by introducing an experiment to compare the amount of unintentional pressure according to the structural characteristics of the robot. However, for an experiment that perfectly sets the control variables, a specific method to fix a DOF and prevent sliding is required. This experimental method could be used to design several exoskeletons to be studied in the future.

The knee joint mechanism proposed in this study was

designed for assisting a human knee on the sagittal plane. We did not yet try to exploit a mechanical structure that can fully produce a three-dimensional trajectory of a human knee and applying it to exoskeletal robots. Recently, the three-dimensional kinematic coupling of a human knee is obtained by the fluoroscopic system [22]. It will be challenging to design the joint mechanism and make it simple and lightweight for wearable hardware. However, it must be studied in this field because it can achieve the ultimate misalignment elimination by imitating all movements on each plane that clearly exist. Therefore, future research will implement more advanced knee joint structures through the three-dimensional motion data.

REFERENCES

[1] H. Iwaki, V. Pinskerova, and M. Freeman, "Tibiofemoral movement 1: the shapes and relative movements of the femur and tibia in the unloaded cadaver knee," *The Journal of bone and joint surgery. British volume*, vol. 82, no. 8, pp. 1189–1195, 2000.

[2] A. B. Zoss, H. Kazerooni, and A. Chu, "Biomechanical design of the berkeley lower extremity exoskeleton (bleex)," *IEEE/ASME Transactions on Mechatronics*, vol. 11, no. 2, pp. 128–138, 2006.

[3] A. M. Dollar and H. Herr, "Design of a quasi-passive knee exoskeleton to assist running," in *Proc. of the 2008 IEEE/RSJ International Conference on Intelligent Robots and Systems*, 2008, pp. 747–754.

[4] M. K. Shepherd and E. J. Rouse, "Design and validation of a torque-controllable knee exoskeleton for sit-to-stand assistance," *IEEE/ASME Transactions on Mechatronics*, vol. 22, no. 4, pp. 1695–1704, 2017.

[5] V. Grosu, C. Rodriguez-Guerrero, S. Grosu, B. Vanderborght, and D. Lefeber, "Design of smart modular variable stiffness actuators for robotic-assistive devices," *IEEE/ASME Transactions on Mechatronics*, vol. 22, no. 4, pp. 1777–1785, 2017.

[6] L. Xie, G. Huang, L. Huang, S. Cai, and X. Li, "An unpowered flexible lower limb exoskeleton: Walking assisting and energy harvesting," *IEEE/ASME Transactions on Mechatronics*, vol. 24, no. 5, pp. 2236–2247, 2019.

[7] Q. Wei, Z. Li, K. Zhao, Y. Kang, and C. Su, "Synergy-based control of assistive lower-limb exoskeletons by skill transfer," *IEEE/ASME Transactions on Mechatronics*, vol. 25, no. 2, pp. 705–715, 2020.

[8] D. Wang, K.-M. Lee, J. Guo, and C.-j. Yang, "Adaptive knee joint exoskeleton based on biological geometries," *IEEE/ASME Transactions on Mechatronics*, vol. 19, no. 4, pp. 1268–1278, 2013.

[9] B. Choi, Y. Lee, J. Kim, M. Lee, J. Lee, S. Roh, H. Choi, Y. Kim, and J. Choi, "A self-aligning knee joint for walking assistance devices," in *Proc. of the 2016 38th Annual International Conference of the IEEE Engineering in Medicine and Biology Society (EMBC)*, 2016, pp. 2222–2227.

[10] Y. Lee, J. Lee, B. Choi, M. Lee, S.-g. Roh, K. Kim, K. Seo, Y.-J. Kim, and Y. Shim, "Flexible gait enhancing mechatronics system for lower limb assistance (gems l-type)," *IEEE/ASME Transactions on Mechatronics*, vol. 24, no. 4, pp. 1520–1531, 2019.

[11] J. Jiang, W. Li, and K.-M. Lee, "A novel pantographic exoskeleton based collocated joint design with application for early stroke rehabilitation," *IEEE/ASME Transactions on Mechatronics*, vol. 25, no. 4, pp. 1922–1932, 2020.

[12] M. Lee, J. Kim, S. Hyung, J. Lee, K. Seo, Y. J. Park, J. Cho, B. k. Choi, Y. Shim, and H. Choi, "A compact ankle exoskeleton with a multiaxis parallel linkage mechanism," *IEEE/ASME Transactions on Mechatronics*, vol. 26, no. 1, pp. 191–202, 2021.

[13] M. Kordasz and P. Sauer, "Automatic determination of knee kinematics for lower limb rehabilitation manipulator design," in *Proc. of the 9th International Workshop on Robot Motion and Control*, 2013, pp. 86–91.

[14] D. J. Hyun, H. Park, T. Ha, S. Park, and K. Jung, "Biomechanical design of an agile, electricity-powered lower-limb exoskeleton for weight-bearing assistance," *Robotics and Autonomous Systems*, vol. 95, pp. 181–195, 2017.

[15] B. Xiao, Y. Shao, and W. Zhang, "Design and optimization of single-degree-of-freedom six- bar mechanisms for knee joint of lower extremity exoskeleton robot," in *Proc. of the 2019 IEEE International Conference on Robotics and Biomimetics (ROBIO)*, 2019, pp. 2861–2866.

[16] Y. Sun, W. Ge, J. Zheng, and D. Dong, "Design and evaluation of a prosthetic knee joint using the geared five-bar mechanism," *IEEE Transactions on Neural Systems and Rehabilitation Engineering*, vol. 23, no. 6, pp. 1031–1038, 2015.

[17] X. Liu and Q. Wang, "Real-time locomotion mode recognition and assistive torque control for unilateral knee exoskeleton on different terrains," *IEEE/ASME Transactions on Mechatronics*, vol. 25, no. 6, pp. 2722–2732, 2020.

[18] H. Terada, Y. Zhu, K. Horiguchi, M. Nakamura, and R. Takahashi, "Development of a wearable assist robot for walk rehabilitation after knee arthroplasty surgery," in *Advances in Mechanisms Design*. Springer, 2012, pp. 65–71.

[19] K. Makino, T. Ogura, M. Nakamura, and H. Terada, "Development of a switchable wearable robot for rehabilitation after surgery of knee," in *Proc. of the Symposium on Robot Design, Dynamics and Control*. Springer, 2020, pp. 60–67.

[20] S. Kuitunen, P. V. Komi, and H. Kyröläinen, "Knee and ankle joint stiffness in sprint running." *Medicine and science in sports and exercise*, vol. 34, no. 1, p. 166, 2002.

[21] K. Kong and M. Tomizuka, "A gait monitoring system based on air pressure sensors embedded in a shoe," *IEEE/ASME Transactions on Mechatronics*, vol. 14, no. 3, pp. 358–370, 2009.

[22] Y.-J. Koo and S. Koo, "Three-dimensional kinematic coupling of the healthy knee during treadmill walking," *Journal of Biomechanical Engineering*, vol. 141, no. 8, 2019.

Taeyeon Kim received the B.S. degree from the Department of Mechanical Engineering, Korea Advanced Institute of Science and Technology (KAIST), Daejeon, Republic of Korea and is currently working toward the M.S. degree in mechanical engineering. His current research interests include hardware design and system control of wearable robots for assistance.

Mingoo Jeong received the B.S. degree in Division of Robotics from Kwangwoon University, Seoul, South Korea, in 2018, the M.S. degree in mechanical engineering from Sogang University in 2020. He is currently working toward the Ph.D. degree in mechanical engineering from Korea Advanced Institutes of Science and Technology (KAIST). His research interests include wearable robotics for assistance, control theory, and general mechatronics.

Kyoungchul Kong received the B.Eng. degree (summa cum laude) in mechanical engineering, the B.S. degree in physics in 2004, and the M.S. degree in mechanical engineering in 2006 from Sogang University, Seoul, Korea, and the Ph.D. degree in mechanical engineering from the University of California at Berkeley, CA, USA, in 2009, where he later became a Postdoctoral Research Fellow until 2011.

In 2011, he joined the Department of Mechanical Engineering, Sogang University, as an assistant professor. He is currently an associate professor of the Department of Mechanical Engineering, Korea Advanced Institute of Science and Technology (KAIST). He is a founder and the CEO of Angel Robotics, a start-up company for productizing wearable robots.

Dr. Kong received the Best Innovation Award from the President of South Korea in 2017, the Commendation by the Minister of Commerce, Industry and Energy in 2017, the Bronze Medal of Cybathlon 2016, the Young Researcher Award of IFAC Mechatronics TC in 2016, the Gold Medal and Bronze Medal of Cybathlon 2020, and many others.